Published in final edited form as:
Phys Rev Lett. 2009 March 20; 102(11): 118102.

Critical buckling length *vs.* persistence length: What governs a biofilament conformation?

Sirish Kaushik Lakkaraju and **Wonmuk Hwang***
Department of Biomedical Engineering, Texas A&M University College Station, TX 77843, U.S.A.

Abstract

We numerically study the length-dependence in the bending stiffness of α-helices, coiled-coils, and a linear chain model. As the length approaches what we named the critical buckling length l_c, the chain appears to become increasingly more flexible. This is due to weak non-bonded attractions that eventually lead to buckling instability and alter the chain's conformational ensemble. For α-helices and coiled-coils, l_c is well less than half of their respective persistence lengths, so l_c is the defining length scale for their conformations. These results elucidate the importance of weak nonspecific attractions that are inherent in many biofilaments in physiological conditions.

Persistence length l_p has been considered as a fundamental length scale that determines the conformation of a uniform chain of length L. Depending on the ratio between L and l_p, the chain conformation can be classified into three regimes; rod-like ($L \ll l_p$), semiflexible ($L \sim l_p$), and flexible ($L \gg l_p$). l_p is determined by the bending stiffness κ of the chain and the temperature T : $l_p = \kappa/k_BT$ (k_B: Boltzmann constant) [1]. It is typically assumed that κ under a given solvent condition is constant, so is l_p. For many biofilaments, l_p has been experimentally measured, including DNA (53 nm) [2], intermediate filaments (1 μm) [3], F-actin (17 μm) and microtubule (5.2 mm) [4]. Atomistic simulations have also been used to calculate l_p, *e.g.*, α-helix (AH; 80−100 nm) [5], coiled-coil (CC; 150−300 nm) [6], and amyloid-like β-sheet filaments (1.2−4.8 μm) [7]. However, l_p depends on L in certain cases, *e.g.*, due to shearing or sliding among protofilaments in microtubules or in intermediate filaments [3,8].

Here we show that length dependence of l_p may be a general feature of biofilaments due to weak nonspecific attractions that are not screened in physiological conditions. In particular, attraction introduces a temperature-independent length scale, the *critical buckling length* l_c, beyond which the chain fails to remain straight. When $l_c < l_p$, l_c rather than l_p governs the filament conformation, which we find to be valid for AHs and CCs.

In the rod regime, normal mode analysis (NMA) can be used to obtain κ. It has been applied to CCs [6], β-sheet filaments [7], and DNA [9]. Yet, the length dependence of κ has not been previously addressed. NMA of an elastic rod yields vibrational bending frequencies ω_n (n = 1,2,3· · ·) that satisfy [10]

$$\kappa=\rho_l\omega_n^2k_n^{-4}, \tag{1}$$

where ρ_l: linear mass density and the wave number $k_n = c_n/L$, where the constant c_n depends on the boundary condition. When both ends of the rod move freely, c_n is the solution of cos

* Electronic address: hwm@tamu.edu.

$c_n \cosh c_n = 1$ [7]. For a perfectly linear elastic rod, κ is independent of n and L. However, for atomistic biofilaments, κ depends on both, and decreases for large L.

To study the length dependence of κ, we performed NMA on straight AHs of various lengths and sequences. We also tested straight leucine-zipper CCs (LZ) with ideal heptad repeats. A straight conformation is required for Eq. (1) to be valid [10]. AHs were constructed by setting the backbone dihedral angles to standard values. We built the backbone of straight LZ using the code by Offer [11] and side chains were placed based on the Protein Data Bank (PDB) structure 2ZTA to ensure a good knob-into-hole packing [12]. The filaments were then energy minimized using CHARMM [13]. A few different minimization schemes did not lead to any noticeable difference in the result.

We used the NMA facility in CHARMM to calculate ω_n. There are twist and stretch modes as well, but we consider only bending modes, which are the most relevant to the chain conformation. $\kappa(L)$ determined from Eq. (1) has a bell-shaped profile (Fig. 1). The initial rise of κ for short L is due to the low aspect ratio of the system that renders the continuum rod picture less accurate [9]. For shorter L there is also stronger edge effect whereby fewer atoms interact, contributing to making κ smaller. After the initial rise, κ is relatively constant or peaks, and then drops for longer L. Beyond the length where κ vanishes, ω_n becomes negative, suggesting that the straight rod conformation is unstable for that mode. This occurs first for $n = 1$, subsequently at higher L for $n = 2$ and so on.

The bell-shaped profile of κ was observed over a range of amino acid sequences in different solvation environments. For AH, we tested poly-alanine (poly-Ala), poly-glycine (poly-Gly), poly-leucine (poly-Leu), and poly-lysine (poly-Lys), either in vacuum (VAC) or in a distance-dependent dielectric (RDIE) medium that mimics the solvation effect, all of which showed bell-shaped profiles. In the plateau region, κ is roughly similar among AHs tested, except for poly-Gly, which gives a smaller value (Fig. 1a,b). Insensitivity of κ on the amino acid sequence of AH agrees with a previous report [5]. Some of these AHs may not fold or are unstable in solution (*e.g.*, poly-Gly). However, in folded forms, their elastic properties (~curvature of the energy well) are mainly governed by the directional and short-ranged backbone hydrogen bond network that forms the *elastic core* of the filament [7]. Side chain interactions determine thermal stability of the structure (~depth of the energy well). This is reflected by the κ of poly-Gly AH being comparable to those of others despite having no side chains (*cf.*, Fig. 4). There is a stronger dependence on the solvation model; κ is nearly twice larger in VAC than in RDIE. In VAC, slower decaying electrostatic interactions in backbone hydrogen bonds render AHs stiffer. For LZ, since they are more stable in solvated environments, we used the ACE2 continuum solvent model in CHARMM [14] that captures the solvation effect better.

The drop of κ for longer chains is due to weak non-bonded attractions among atoms that increase as the chain bends and eventually lead to buckling instability. To check, we constructed a bead on a chain model (*1D chain*) where beads have the mass of a carbon atom, and are connected by harmonic springs of rest length $b = 1$ Å and spring constant $K_b = 8000$ kcal/mol·Å^2 (unless otherwise noted). Bending stiffness is prescribed by a harmonic potential for the bond angle θ, $U(\theta) = K_\theta(\theta - \pi)^2$, with $K_\theta = 800$ kcal/mol·rad^2 (unless otherwise noted). Non-bonded attraction is incorporated via the Lennard-Jones potential for the distance r between any two non-neighbor beads

$$V_{LJ}(r) = \epsilon\left[(2b/r)^{12} - 2(2b/r)^6\right]. \quad (2)$$

NMA shows that when $\varepsilon = 0$, κ does not drop, which also agrees with the analytic expression $\kappa = 2b\left(1 - \frac{b}{L}\right)K_\theta$ (Fig. 1d). κ drops for $\varepsilon = 0.3$ kcal/mol and further for $\varepsilon = 0.7$ kcal/mol, confirming that the drop is indeed due to the attractive force. In the plot of log ω_1 *vs.* log L, deviation of the slope from −2 occurs at smaller L for larger ε (Fig. 2a).

Although NMA efficiently characterizes biofilament elasticity [6,7,9], it uses a harmonic approximation around the conformational energy minimum. To check if the drop in κ also occurs without the harmonic approximation, we performed thermal motion analysis (TMA) [7] whereby l_p (hence κ) is estimated by applying the worm-like chain model to the end-to-end distance R [15]

$$\left\langle R^2 \right\rangle = 2l_p\left[L + l_p\left(e^{-L/l_p} - 1\right)\right], \tag{3}$$

where $\langle R^2 \rangle$ is the time average. We performed Langevin dynamics simulations on the 1D chain at 300 K, with $\varepsilon = 440$ kcal/mol, $K_b = 4000$ kcal/mol·Å^2 and $K_\theta = 400$ kcal/mol·rad^2. We tested the range $L = 29$−119 Å for several hundred nanoseconds. Drop in κ again occurred (Fig. 1d). However, κ measured in TMA with $\varepsilon = 0$ did not show a drop (data not shown).

Remarkably, when we calculated κ from the variance of θ along the chain and by applying the equipartition theorem, no drop was observed (Fig. 2b). Similarly, we performed molecular dynamics (MD) simulations of poly-Ala in VAC for 20 ns, and measured κ using a local fluctuation analysis developed in [5], which did not show a drop. On the other hand, TMA of the same MD trajectories did show a drop in κ for longer AHs (Fig. 2b). We observed a similar behavior in MD simulations of AHs constructed using the sequence of the single α-helix (SAH) domain of myosin X [23], which remained folded in the ACE2 continuum solvent environment (data not shown). Note that even when the apparent κ obtained from global analyses (NMA or TMA) is small, the chain does not collapse (Fig. 2c). Therefore, longer chains do not actually become locally flexible. Instead, weak attractions alter their conformational ensemble, and make them appear to be more flexible.

To additionally check our calculation, we performed an explicit-water MD simulation of a 44-Å poly-Ala AH for 3.1 ns. While the simulation time was too short to apply TMA, local fluctuation analysis as above [5] yielded $\kappa = 3.5 \times 10^{-28}$ Nm^2, slightly above the plateau value in RDIE (*cf.*,Fig. 4). For LZ, we performed the 'forced bending' simulation where a transverse force was incrementally applied at the free end of a cantilevered LZ [7]. It remained linearly elastic up to a 32.9% strain, and gave κ similar to those from NMA (Fig. 1c).

Above results suggest that non-bonded attraction cannot be ignored for sufficiently long filaments. Even when forces balance in a straight configuration, attraction between two points on the chain increases as it bends. As non-bonded attraction is usually weak, restoring force prevails for short chains. However, beyond a certain length, the filament develops buckling instability, which can be described as [10]

$$\rho_l \omega_n^2 = k_n^2\left(\kappa_0 k_n^2 - f_c\right), \tag{4}$$

where κ_0 is the length-independent, local bending stiffness. The critical buckling force f_c represents non-bonded attraction. Setting $f_c = 0$ in Eq. (4) restores Eq. (1). Since $k_n = c_n/L$, for a given f_c,

$$l_c = c_n \sqrt{\kappa_0 / f_c}, \quad (5)$$

such that for $L > l_c$, $\omega_n^2 < 0$, *i.e.*, there is no stable wave solution. Since c_n grows with n, higher modes have larger l_c, as in Fig. 1. Using Eq. (4), we replot the data with $X \equiv L^{-2}$ *vs.* $Y \equiv \omega_n^2 L^2$ (Fig. 3). From the linear fit, κ_0, f_c, and l_c can be retrieved (Fig. 4). κ_0 thus retrieved is indeed close to the plateau value of $\kappa(L)$ in Fig. 1.

While we address the length dependence of κ, for a given L, our results agree favorably with previous ones. A local fluctuation analysis of 78-residue (113 Å) long poly-Ala AH yielded $\kappa = 4.91 \times 10^{-28}$ Nm^2 in VAC [5], while we get $(5.44–5.65)\times 10^{-28}$ Nm^2. As for CC, a previous study of the myosin S2 domain (PDB 1NKN, 76 residues) reports $\kappa = 7.20\times 10^{-28}$ Nm^2 [6]. This was measured on a bent structure, with the end to end distance (96 Å) used for L. But Eq. (1) applies only to straight rods. Upon rebuilding a straight CC using the S2 sequence (L = 105 Å), we get $\kappa = 10.9 \times 10^{-28} \approx (105/96)^4 \times 7.20 \times 10^{-28}$ (Nm^2) (*cf.*,Eq. (1)). Also, residues 106 −224 of tropomyosin CC (L = 168 Å; from PDB 2B9C) has $\kappa = 9.22 \times 10^{-28}$ Nm^2. In contrast, a 84-residue LZ (L = 121 Å; rise phase in Fig. 1c) has $\kappa = 14.3 \times 10^{-28}$ Nm^2. Higher stiffness of LZ may be attributed to the good knob-into-hole packing of side chains that contribute to its elastic core. This was further tested on cortexillin [16], a stiff CC (PDB 1D7M, L = 146 Å): $\kappa = 15.2 \times 10^{-28}$ Nm^2, comparable to a LZ with a similar length. Compared to AH, stiffness of CC thus has a stronger sequence-dependence.

From the NMA of myosin S2 and the fragment of tropomyosin considered above, we get l_p as 260 nm and 223 nm, respectively, which are 1.8 to 3.5 times longer than experimental estimates [17-19]. As irregularities in the heptad periodicity may locally destabilize the molecule [20, 21], our calculation based on completely folded CCs in ACE2 provides an upper bound of l_p. Previously, mechanical properties of a single AH and the CC geometry were used to estimate $l_p \simeq$ 150 nm [22]. The smaller value in this continuum rod model may be because the deformation-dependence of energy by the knob-into-hole packing was ignored.

An important outcome of the present work is that for AHs and CCs, $l_c < l_p$ (Fig. 4), suggesting that l_c rather than l_p is the length scale governing the chain conformation. In cases when an AH or a CC need to remain straight, they should be shorter than l_c (~12 nm for AH and <~70 nm for CC). A good example is the SAH domain of myosin X (L = 5.3 nm), that forms a part of the lever arm [23]. Also, the 50-nm long CC stalk of kinesin has a hinge in the middle [24], so that the respective CC segments are well shorter than l_c.

As long as there is non-bonded attraction, filaments buckle for $L \geq l_c$. For thin flexible polymers (*e.g.*, polystyrene), l_p is only several chemical bonds in length. In this case, non-bonded attraction can be easily offset by changing the solvent quality, where the distinction between good and poor solvent regimes is well-established [25]. Biofilaments are stiffer, with l_p far greater than the chemical bond length or the size of solvation shells around polar groups of the chain (a few Å). Hence, changes in solvent quality is not as effective in canceling attractive forces. Furthermore, non-bonded attraction, which is typically the van der Waals force, is screened little in physiological conditions, in contrast to Coulombic forces [26]. Attraction-induced critical buckling should thus be more relevant to biofilaments. However, other interactions may come into play. Strong negative charges on DNA may generate repulsive forces that offset the weak attraction, making it difficult to observe buckling instability. Longer microtubules appear to be stiffer, although the study in [8] tested L in the range of $0.1 l_p$ and does not preclude buckling for longer L. It would be interesting to see if l_c is less than l_p in F-actin, which has only two protofilaments and the shearing effect may not be as pronounced as in microtubules.

Since l_c is temperature independent (other than through κ_0 and f_c that may have weak T-dependence), the $L > l_c$ regime is not in conformational equilibrium and the chain will be trapped in a subset of conformations that may depend on the way how the system is prepared. In the case of a polymer network, the importance of attractive interaction has been previously considered: no matter how small, due to abundant contacts among polymers, nonspecific attractions eventually lead to non-equilibrium or glassy behavior [25,27]. The present work shows that, even for a single biofilament, weak attractive force can profoundly affect its conformation.

Acknowledgments

We acknowledge Gerald Offer for providing the CC-building code. This work was supported by the National Institute of Health (Grant number: R21NS058604).

References

1. Howard, J. Mechanics of Motor Proteins and the Cytoskeleton. Sinauer Associates, Inc; 2001.
2. Rivetti C, Guthold M, Bustamante C. J. Mol. Biol 1996;264:919. [PubMed: 9000621]
3. Mücke N, Kreplak L, Kirmse R, Wedig T, Herrmann H, Aebi U, Langowski J. J. Mol. Biol 2004;335:1241. [PubMed: 14729340]
4. Gittes F. J. Cell Biol 1993;120:923. [PubMed: 8432732]
5. Choe S, Sun SX. J. Chem. Phys 2005;122:244912. [PubMed: 16035821]
6. Adamovic I, Mijailovich S, Karplus M. Biophys. J 2008;94:3779. [PubMed: 18234833]
7. Park J, Kahng B, Kamm RD, Hwang W. Biophys. J 2006;90:2510. [PubMed: 16415051]
8. Pampaloni F, Lattanzi G, Jonas A, Surrey T, Frey E, Florin E. Proc. Natl. Acad. Sci. USA 2006;103:10248. [PubMed: 16801537]
9. Matsumoto A, Go N. J. Chem. Phys 1999;110:11070.
10. Landau, LD.; Lifshitz, EM. Theory of Elasticity. Vol. 3rd ed.. Pergamon Press; 1986.
11. Offer G, Sessions R. J. Mol. Biol 1995;249:967. [PubMed: 7791220]
12. Crick FHC. Acta Crystallographica 1953;365
13. Brooks B, Bruccoleri R, Olafson B, States D, Swaminathan S, Karplus M. J. Comp. Chem 1983;4:187.
14. Schaefer M, Karplus M. J. Phys. Chem 1996;100:1578.
15. Marko J, Siggia E. Macromolecules 1995;28:8759.
16. Burkhard P, Kammerer R, Steinmetz M, Bourenkov G, Aebi U. Structure 2000;8:223. [PubMed: 10745004]
17. Hvidt S, Nestler FHM, Greaser ML, Ferry JD. Biochemistry 1982;21:4064. [PubMed: 7126531]
18. Uyeda T, Abramson P, Spudich J, Howard J. Proc. Natl. Acad. Sci. USA 1996;93:4459. [PubMed: 8633089]
19. Phillips G Jr, Chacko S. Biopolymers 1996;38:89. [PubMed: 8679944]
20. Brown J, Cohen C, Parry D. Proteins 1996;26:134. [PubMed: 8916221]
21. van Noort J, van der Heijden T, de Jager M, Wyman C, Kanaar R, Dekker C. Proc. Natl. Acad. Sci. USA 2003;100:7581. [PubMed: 12805565]
22. Wolgemuth C, Sun S. Phys. Rev. Lett 2006;97:248101. [PubMed: 17280328]
23. Knight P, Thirumurugan K, Xu Y, Wang F, Kalverda A, Stafford W III, Sellers J, Peckham M. J. Biol. Chem 2005;280:34702. [PubMed: 16030012]
24. de Cuevas M, Tao T, Goldstein L. J. Cell Biol 1992;116:957. [PubMed: 1734025]
25. de Gennes, P-G. Scaling Concepts in Polymer Physics. Cornell University Press; Ithaca, NY: 1979.
26. Israelachvili, JN. Intermolecular and Surface Forces. Vol. 2nd ed.. Academic Press; 1992.
27. Fabry B, Maksym G, Butler J, Glogauer M, Navajas D, Fredberg J. Phys. Rev. Lett 2001;87:148102. [PubMed: 11580676]

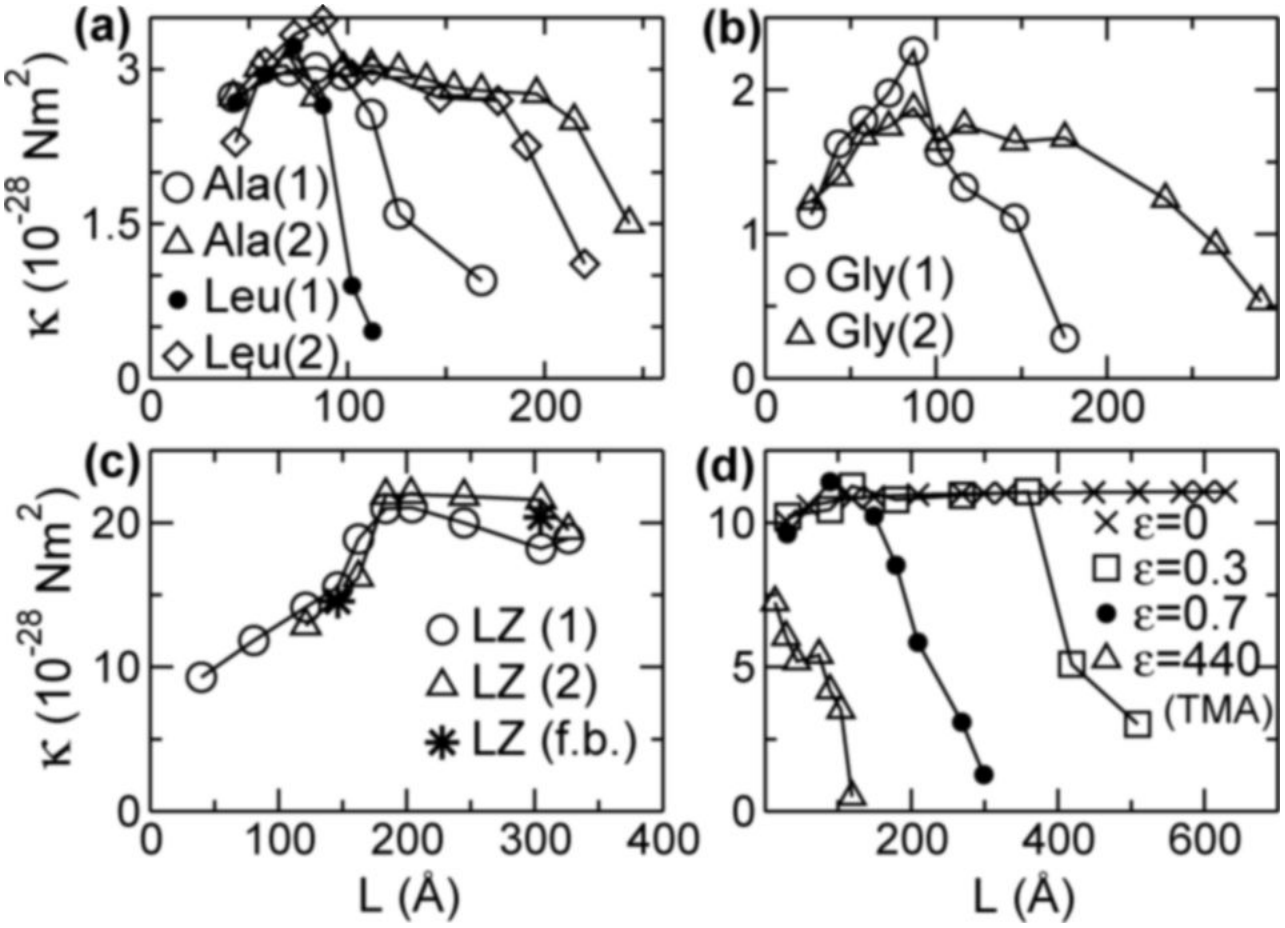

FIG. 1.

κ vs. L. (a) Poly-Ala, poly-Leu, and (b) poly-Gly AHs, (c) LZ, and (d) 1D chain (ε in units of kcal/mol). All are from NMA (n = 1, 2, in parentheses; and n = 1 in (d)), except (c) f.b.: forced-bending simulation, (d) TMA for ε = 440. Solvent models used are: (a,b,d) RDIE, and (c) ACE2 [14]. Similar plots are obtained for AHs in VAC, with κ overall larger (*cf*., Fig. 4). κ further dropped for LZ at 487 Å, but is not plotted since the chain bent slightly during the initial energy minimization.

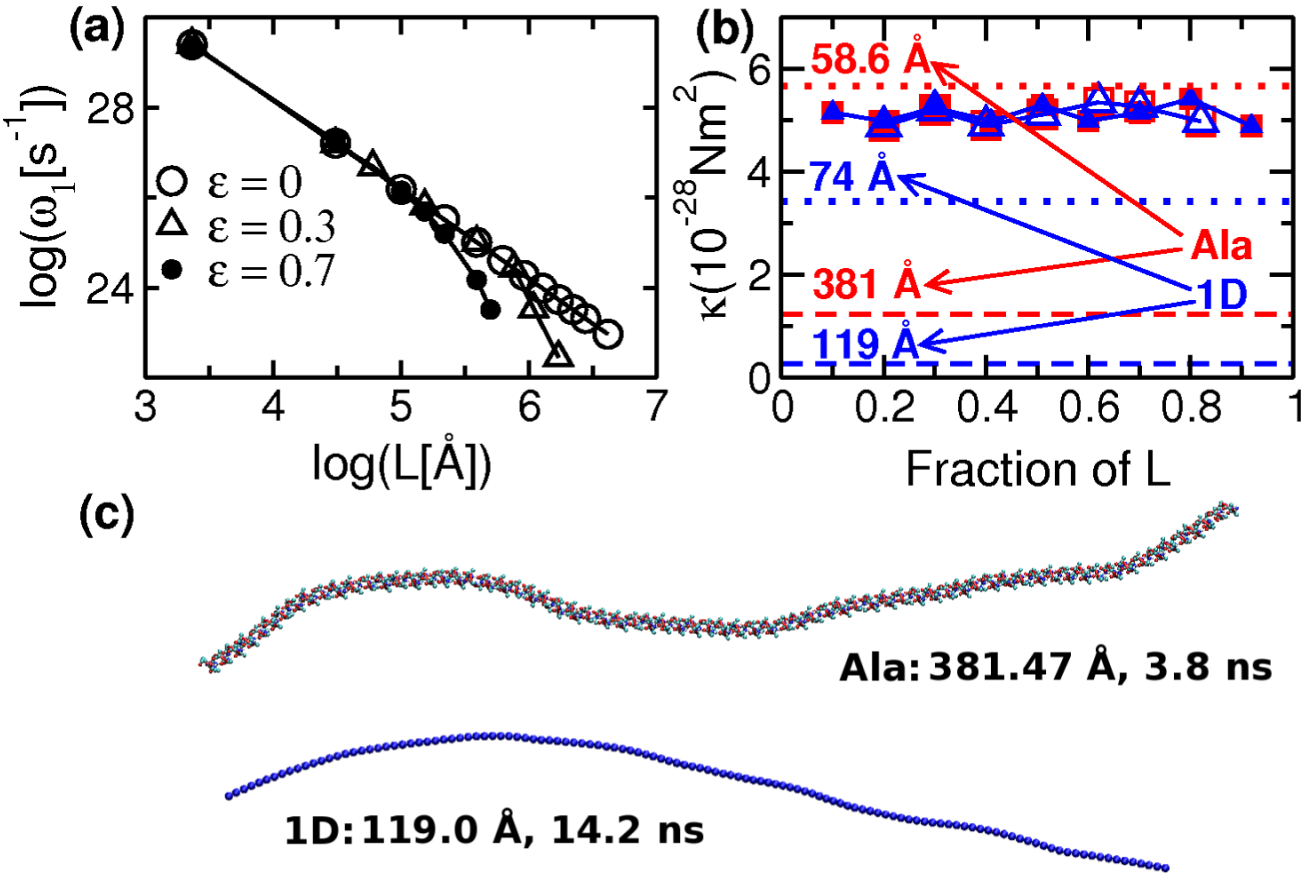

FIG. 2.

(Color online). Whole-chain analysis (NMA and TMA) *vs*. local fluctuation analysis. (a) Deviation from linear elasticity in 1D chain, occurring from shorter L for larger ε. (b) Symbols: κ obtained from local fluctuation analysis, which are independent of L. Square: AH (in VAC; open: 58.6 Å, solid: 381 Å), Triangle: 1D chain (ε = 440; open: 74 Å, solid: 119 Å). Dashed and dotted horizontal lines: κ obtained from TMA, which decreases with L. (c) Sample snapshots of long chains during MD, which do not collapse.

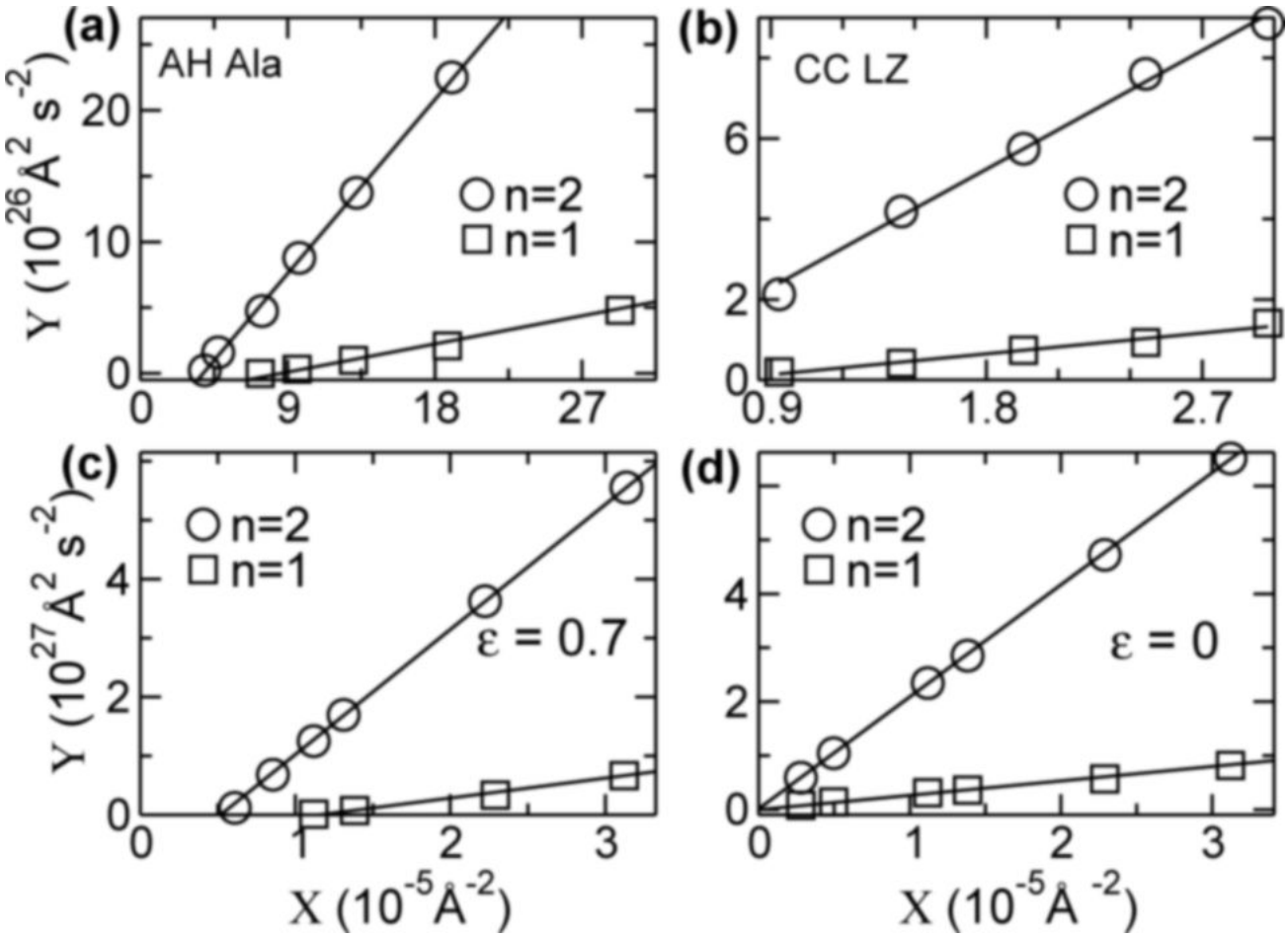

FIG. 3.

$X - Y$ plot ($X \equiv L^{-2}$, $Y \equiv \omega_n^2 L^2$). Solid line: linear fit. The initial rise phase in Fig. 1 was not used in the fit. Only portions near the origin are shown. In (d), lines converge to the origin, hence $f_c \approx 0$.

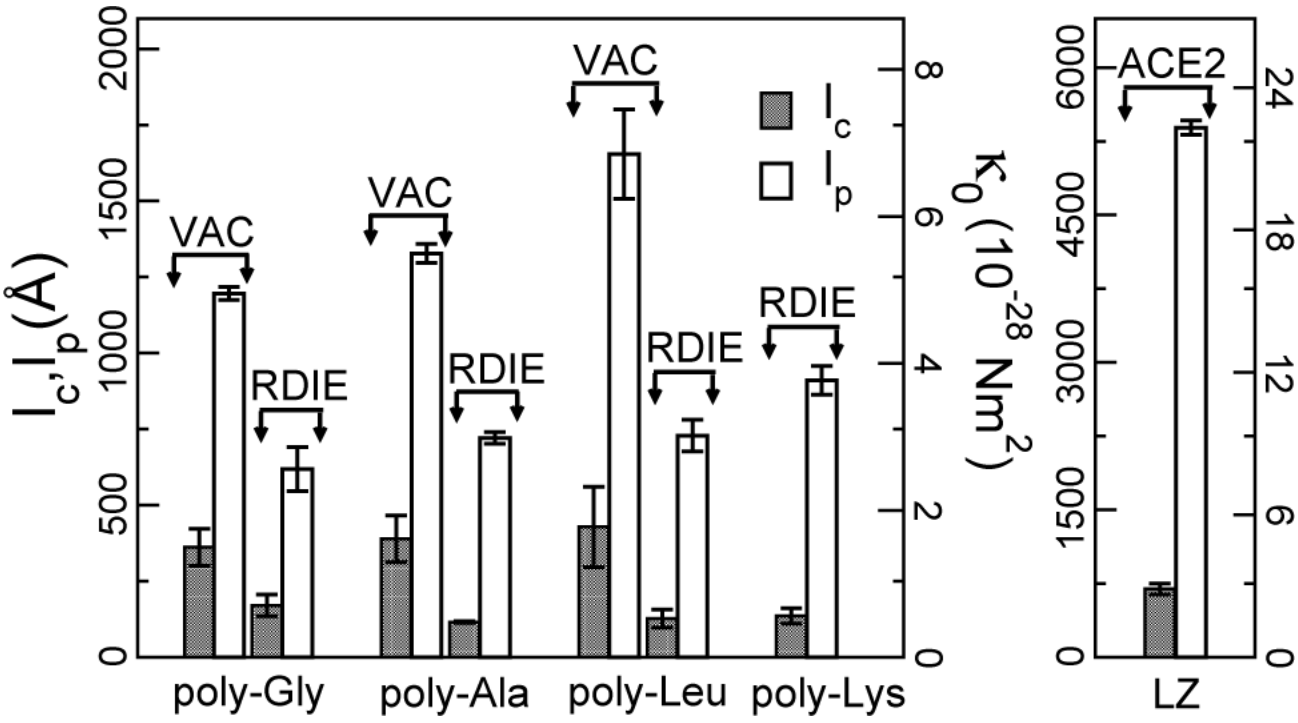

FIG 4.

l_c, l_p, and κ_0 of AH and LZ determined from the $X - Y$ plots for $n = 1$ (Fig. 3). For LZ, labels of the y-axes follow those of AH on respective sides.